

# Towards Self-Supervised Category-Level Object Pose and Size Estimation

Yisheng He<sup>1</sup> Haoqiang Fan<sup>2</sup> Haibin Huang<sup>3</sup> Qifeng Chen<sup>1</sup> Jian Sun<sup>2</sup>

<sup>1</sup>Hong Kong University of Science and Technology <sup>2</sup>Megvii Technology <sup>3</sup>Kuaishou Technology

## Abstract

This work presents a self-supervised framework for category-level object pose and size estimation from a single depth image. Unlike previous works that rely on time-consuming and labor-intensive ground truth pose labels for supervision, we leverage the geometric consistency residing in point clouds of the same shape for self-supervision. Specifically, given a normalized category template mesh in the object-coordinate system and the partially observed object instance in the scene, our key idea is to apply differentiable shape deformation, registration, and rendering to enforce geometric consistency between the predicted and the observed scene object point cloud. We evaluate our approach on real-world datasets and find that our approach outperforms the simple traditional baseline by large margins while being competitive with some fully-supervised approaches.

## 1. Introduction

Category-level pose and size estimation is an important requirement in various real-world applications, such as autonomous driving [12, 7, 44], augmented reality [27], and robotic manipulation [8, 33, 14]. The goal of this task is to predict the 9D translation, orientation and size of novel objects in the same category. Contrary to instance-level pose estimation [14, 13] for seen objects with CAD models, category-level algorithms are required to handle various objects within the same category and generalize to novel objects in inference. The intra-class variation of objects' shape and color makes this new problem more challenging.

Recently, with the development of deep learning techniques, various data-driven approaches [38, 32, 6] have been introduced to tackle the problem and achieve significant improvement over traditional algorithms [1]. Since no instance-level object CAD models are provided to serve as the reference frame, two kinds of representation are introduced to define the category-level pose and size. One line of works [38, 4] utilize implicit Normalized Object Coordinate Space (NOCS) to map all possible object instances into the same representation. Specifically, objects in the same class

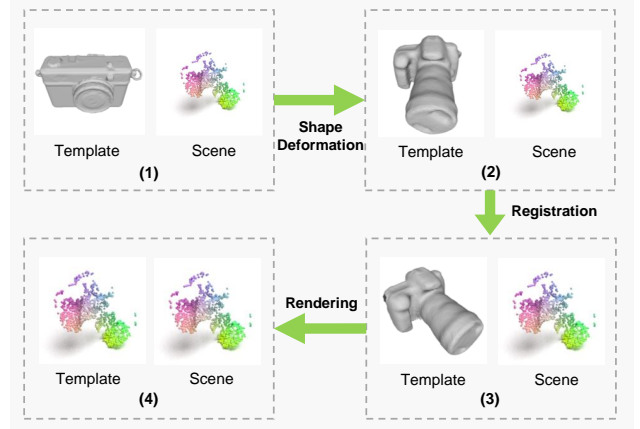


Figure 1: Challenges to self-supervised category-level pose and size estimation reside in the entangled shape, pose, scale, and partial-to-complete inconsistencies between the category template mesh and scene point cloud, shown in (1). We leverage differentiable shape deformation, registration, and rendering to disentangle them step by step and enforce geometric consistency between the rendered and observed scene point clouds for self-supervised learning.

are normalized to the same size and orientation for a unified representation. However, explicit shape variations of different objects in the same category are lost in such representation, which limits the performance of pose estimation. More recent works [32, 5], instead, represent a category of objects by a normalized prior shape, which is then deformed to obtain the exact shape of novel objects for particular pose and size estimation.

Despite compelling results being achieved, existing data-driven approaches heavily rely on large-scale datasets with ground truth pose labels for fully-supervised learning. Unlike many 2D vision tasks, i.e., classification and segmentation, acquiring real-world 6D pose annotations is much more labor-intensive and error-prone [15, 20, 37], which hinders learning-based algorithms from scaling up. On the other hand, large-scale unlabeled depth data becomes easy to obtain with the rising prevalence of depth sensors, which provokes us to consider an interesting research question:

How to leverage this data for self-supervised learning of category-level object pose and size estimation?

In this work, we propose a novel self-supervised framework for label-free pose and scale estimation. Given the category template mesh, our key idea is to leverage differentiable shape deformation, registration, and rendering to enforce the *geometric consistency* between the rendered and the observed object point cloud for self-supervision. As shown in Figure 1, challenging obstacles to this idea resides in the entangled shape, pose, scale, and partial-to-complete inconsistency between the observed point cloud and the category template mesh. To path the way, we first introduce a pose- and scale-invariant shape deformation network to deform the template mesh to the target shape and eliminate the shape inconsistency. This module is weakly supervised by a complete coarse point cloud of the target object in the same pose and scale as the template mesh. Then, taking points sampled from the deformed mesh and the observed scene, a partial-to-complete registration network is applied for pose and scale estimation. Finally, with the predicted pose and scale parameters, we scale and transform the deformed mesh to the scene and leverage a differentiable renderer to render the visible part and eliminate the partial-to-complete inconsistency. In this way, we can enforce the *geometric consistency* between point clouds lifted from the rendered depth and the observed scene for self-supervision of pose and scale estimation.

We further conduct experiments on real-world datasets to validate the proposed approach. Experimental results show that our approach outperforms the traditional baseline significantly while competitive with some full-supervised approaches.

To summarize, the main contributions of this work are:

- A novel self-supervised framework for category-level object pose and size estimation via differentiable shape deformation, registration, and rendering;
- A novel pose- and scale-invariant mesh deformation network and a multi-scale geometry enhancement mechanism that fully leverages local and global geometric information for deformation guidance;
- Extensive experiments demonstrate the efficacy of our approach against traditional and supervised category-level pose and size estimation approaches;
- In-depth analysis to understand various design choices of our system.

## 2. Related Work

### 2.1. Fully-Supervised Category-Level Pose and Size Estimation

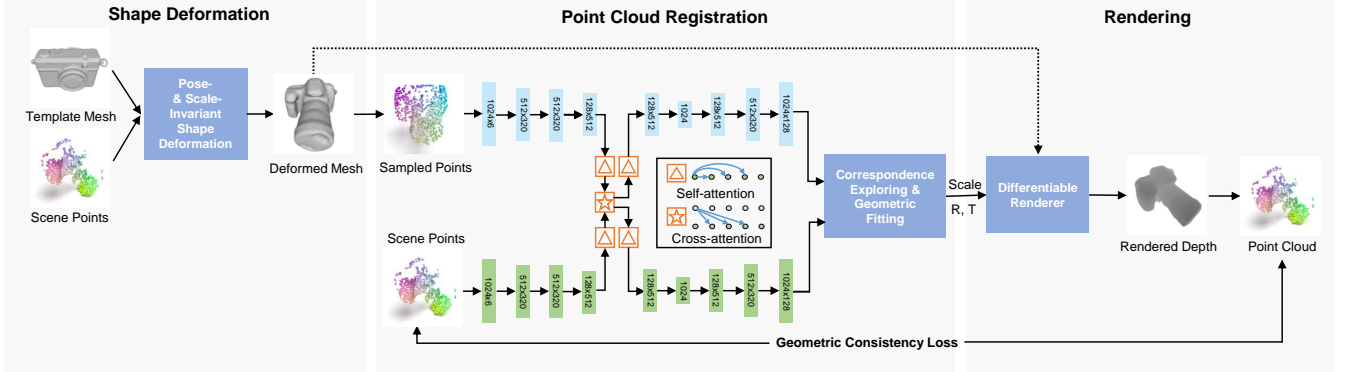
NOCS-based approaches [38, 4] utilize normalized object coordinate space to represent objects within the same category for pose estimation. Shape-Prior based [32, 39, 5] jointly deform category-level prior point clouds and establish dense correspondence to recover pose parameters. Direct regression approaches [6, 25] are also introduced to the problem. However, these algorithms heavily rely on the labor-intensive ground truth pose annotations for training.

### 2.2. Self-Supervised Pose Estimation

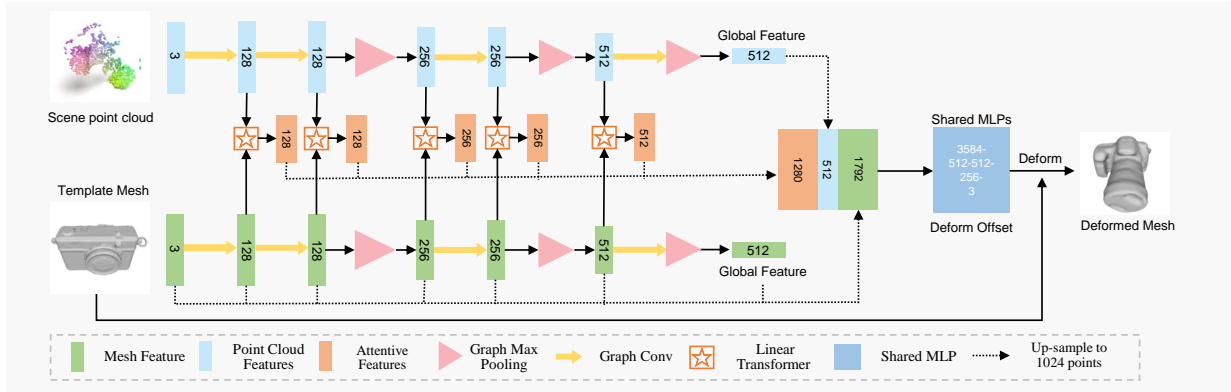
Given its practical importance, several works have looked into applying self-supervised techniques for *instance-level* pose estimation. [37, 31] fine-tunes pre-trained model from synthesis data on real data through visual and geometric alignment. However, the reliance on precise instance-level object CAD model hinders the application of these frameworks to the *category-level* problem. Concurrently with our work, [24] leverage SE(3) equivariance point cloud network for joint point shape reconstruction and 6D pose estimation. However, they ignore the 3D size parameters and focus on rotation and translation estimation. While the 3D size information is useful in many real-world applications (i.e., robot manipulation), our work targets the more challenging 9D pose and size estimation. Besides, before being applied to real-world data, existing works [24, 37, 31] require large-scale synthesis data rendered from precise CAD models for network pre-training. While collecting precise object CAD models for new categories is labor-intensive, our framework is designed to be directly optimized on real-world data. To the best of our knowledge, we are the first to propose a self-supervised category-level *pose* and *size* estimation framework that can be directly optimized on unlabeled real depth images without any pre-training.

### 2.3. Shape Deformation

Shape deformation techniques are applied for object reconstruction from single images or point clouds. Learning-based algorithms can be divided into volumetric warps [18, 23, 46, 22], cage deformations [45], vertex-offsets-based [41] and flow-based approaches [19]. Most related to our work, 3DN[41] regresses vertex offsets to deform mesh from global features extracted from the source meshes and target point clouds. However, it assumes small pose and scale differences and are sensitive to such variations. Similar to ours, FS-Net [6] utilizes shift and scale-invariant 3DGCN to extract global features for oriented point cloud reconstruction. However, the reconstructed points are sparse without topology information, causing artifacts in



(a) **The overall pipeline of our framework.** Our pipeline consists of three main steps. Firstly, a pose- and scale-invariant shape deformation network is utilized to deform the template mesh to the shape of the observed object. Then, a point cloud registration network is applied to explore correspondence and estimate the pose and scale parameters. Finally, the deformed mesh is rendered by a differentiable renderer and the geometric consistency between the rendered and the observed scene point cloud is established for self-supervised learning.



(b) **The pose- and scale-invariant shape deformation network.** We apply shift- and scale-invariant 3DGCN [26] for feature extraction. The local and global geometric features of the template mesh along with the pose- and scale-invariant point cloud global feature are directly applied for shape deformation. To fully leverage different levels of local geometric information resides in the partial object point cloud to guide the shape deformation, a novel multi-scale geometry enhancement mechanism based on Linear Transformers [40] is also utilized to extract more geometric details and guide better shape deformation.

Figure 2: Overview of our pipeline.

rendered depths. The orientation of points is not disentangled as well. In contrast, we propose a pose- and scale-invariant framework to extract features for mesh deformation. Moreover, to fully leverage the local and global geometric information from the observed partial point cloud, we introduce a novel multi-scale cross attention module based on transformers to enhance the shape deformation.

### 3. Proposed Method

Given the partial point cloud of a novel object from the scene and its category template mesh, the target is to obtain its 6D pose and 3D size parameters. Though the observed object point cloud and the template mesh are within the same category, they are inconsistent in three dimensions, making the problem challenging. Firstly, they are in different shapes. Secondly, their poses and sizes are different. Lastly, the observed point cloud is partial while the prior mesh model is complete. To design a self-supervised

framework for pose and size estimation, we need to eliminate these inconsistencies to establish consistent constrain for network supervision.

#### 3.1. Overview

As shown in Figure 2(a), we solve the problem in three steps, by differentiable mesh deformation, point cloud registration, and mesh rendering. Each step tackles one of the above inconsistency problems and eventually establishes the geometric consistent constrain between the rendered depth and the observed scene point cloud for self-supervision. Specifically, in the first step, a pose- and scale-invariant shape deformation network is utilized to deform the prior mesh model to the target object s.t. the observed partial point cloud to eliminate the shape inconsistency. Inspired by point cloud registration pipelines [16, 10], in our second step, we estimate pose and size parameters by extracting feature descriptors, finding correspondences, and

estimating the best alignment. Finally, we transform the deformed mesh by the predicted scale and pose to the camera coordinate system and utilize differentiable rendering to eliminate the partial-to-complete inconsistency. The rendered depth map is lifted back to a partial point cloud that should be geometric consistent with the observed scene point cloud, which can serve as the supervision signal to our framework. Each module in our pipeline is differentiable by design, and the whole framework can be optimized end-to-end.

### 3.2. Pose and Scale Invariant Shape Deformation

Given the observed partial point cloud,  $P_{scn}$  of a novel object and its normalized category template mesh,  $M_{tp}$ , our task is to deform  $M_{tp}$  to the target mesh  $M_{tgt}$ , where  $M_{tgt}$  is with the same shape as  $P_{scn}$  while kept in the same pose and scale as  $M_{tp}$ . We represent  $P_{scn} \in \mathbb{R}^{N_P \times 3}$  with  $N_P$  the number of points,  $M_{tp} \in (V, E)$  with  $V \in \mathbb{R}^{N_V \times 3}$  the 3D positions of vertices and  $E \in \mathbb{Z}^{N_E \times 3}$  the set of triangles. As shown in Figure 2(b), taking  $P_{scn}$  and  $V$  as inputs, our network regress the deformation vectors  $D \in \mathbb{R}^{N_V \times 3}$  of each vertex to deform  $M_{tp}$  to the target mesh  $M_{tgt} = (V', E)$ , where  $V' = V + D$ . There are two challenges in this task. Firstly, the template mesh and observed point cloud are in different poses and scales, for which existing works [41, 45] can not handle well by design. Secondly, it remains unknown how to fully leverage the structure and geometric information residing in the observed *partial* point cloud to enhance the mesh deformation. To tackle the first challenge, we introduce a pose- and scale-invariant feature extraction backbone based on a 3DGC (3D graph convolution) network[26]. For the second problem, we propose a novel multi-scale attention module that can fully leverage the local and global geometric information residing in the partial point cloud to enhance mesh deformation.

#### 3.2.1 Pose and Scale Invariant Feature Extraction

We utilize the shift and scale-invariant 3DGC network as our feature extraction backbone to eliminate the pose and scale-invariant. 3DGC network is firstly applied to point cloud classification, object part segmentation [26] and extended to visible point reconstruction in [6]. In this work, we further extend it to the mesh deformation problem. By designed, 3DGC is invariant in shift and scale (see [26] for details). We utilize rotation invariant global max pooling to eliminate the influence of different orientations further to obtain the final pose and scale-invariant global geometric features. Since the template and target mesh are in the normalized coordinate systems with the same pose and scale, we can easily leverage local and global geometric features from the template as geometric prior to deformation. As a guide to target shape deformation, geometric information

from the observed scene point cloud is also required. One simple way is to add the scale- and pose- invariant global geometric feature from the scene point cloud as guidance. However, the global features lose local geometric details in the scene point cloud due to the max-pooling operation. While local geometric details are also helpful to enhance mesh deformation, we propose a novel multi-scale attentive geometry enhancement module to make full use of this information in the following section.

#### 3.2.2 Multi-Scale Geometry Enhancement with Transformers

In the design of the encoder-decoder geometry feature extraction framework, local features are extracted with smaller perspective fields in the early stages. When the network goes deeper, the perspective field grows larger, and more global features are extracted. To guide the shape deformation better, both local and global geometric features from the observed target point cloud are crucial. Precisely, the early local features can guide the deformation of geometry details while the global ones guarantee global topology consistency. However, it is nontrivial to obtain corresponding local features from points in the scene to each vertex in template mesh, as they are not one-to-one aligned. To tackle the problem, we observe that corresponding parts of different object instances within the same category are in similar geometric structures, and the extracted geometric features are also similar. Therefore, we can utilize the similarity between local geometric features of each vertex in template mesh and each point in the scene to obtain the most related local features for deformation guidance. Such formulation is similar to the attention mechanism in Transformers [35, 40], leading to a straightforward choice of using Transformer networks to serve our purpose.

The Transformers first introduced in Natural Language Processing is good at capturing the long-term dependency, even on un-ordered sets. The key element in Transformers is the attention layer. Taking the input vectors, namely query  $Q$ , key  $K$  and value  $V$ , the attention module retrieves information from  $V$  according to the attention weight calculated from the dot product of  $Q$  and  $V$ , i.e.,  $I = softmax(QK^T)V$  with  $I$  the retrieved info. To reduce the quadratic computational cost of vanilla transformers [35], we apply the optimized Linear Transformer [40] to extract the corresponding local geometric features from scene points to enhance features of the template mesh. Specifically, we take local features from the template mesh as  $Q$  and local features from scene points as  $K$  and  $V$  and feed them to the Linear Transformers. The retrieved local geometrical features are then fed into the mesh deformation network header. We apply Linear Transformers on each encoding layer to retrieve multi-scale local to global geometric

information from scene points. Another advantage of this mechanism is that the attention mechanism eases the negative effect of the partial-to-complete inconsistency. Specifically, invisible symmetric parts of the template mesh can also retrieve geometric information from the visible symmetric parts with the attention module to guide deformation.

### 3.3. Differentiable Registration for Pose and Size Estimation

Now we have eliminated the shape inconsistency by our pose- and scale-invariant shape deformation network. In this section, we focus on the pose and size estimation. Given the deformed mesh  $M_{df} = (V', E)$  in the normalized object coordinate space and the observed scene point cloud in the camera coordinate space, our task is to estimate a scale parameter, denoted  $s$  to scale  $M_{df}$  to its actual object size, and a rotation  $R \in SO(3)$  as well as a translation  $T \in SE(3)$  to transform  $M_{df}$  to the camera coordinate system. After this step, the visible part of the scaled and transformed mesh  $M_{df}^{cam} = (V^{cam}, E)$  in the camera coordinate should be aligned with scene points, where  $V^{cam} = sRV' + T$ . Inspired by the success of differentiable registration in the point cloud alignment [10] field, we formulate the problem as point cloud registration but estimate an extra scale parameter. Specifically, we utilize differentiable sampling [41] to sample a point cloud from the surface of the deformed mesh and then align it to the scene point cloud by correspondence exploring and geometric fitting. The correspondence exploring establishes the 3D-3D correspondence between the two point clouds while the geometric fitting estimate pose and scale parameters by Umeyama algorithms [34]. The pipeline is shown in the middle part of Figure 2(a).

#### 3.3.1 Point-wise Feature Extraction & Correspondence Exploring

Before pose and scale estimation, we first establish the correspondence between mesh points and scene points on the geometric features space. As shown in Figure 2(a), we utilize two-point cloud networks, i.e. PointNet++ [28] to extract point-wise features for the two point clouds respectively. Weights on the two PointNet++ are shared to be Siamese. Challenges of this part reside in the partial to complete and the pose and scale inconsistency between the two point clouds. Recently, PREDATOR [16] introduced a deep attention block to enable early information exchange on the final feature encoding layer. Contextual information aggregated in this way better guides robust feature extraction for matching. Specifically, Graph Neural Networks (GNN) [42] are first applied to aggregate contextual relations individually. Then a Transformer network is applied as a cross-attention module to enhance contextual informa-

tion (see more details in [16]). We apply a similar technique but improve it in two ways. Firstly, GNN can only establish local attention with small perspective fields since only  $K$  nearest neighbors are linked to the graph. Therefore, we replace it with Linear Transformers that are good at capturing long-term dependency to establish global attention for better contextual aggregating. Secondly, in the cross attention part, we replace the vanilla transformers [16] with Linear Transformers to reduce the computational cost.

After local feature extraction, we obtain point-wise features for each points on the two point cloud. We can establish the correspondences between the them by finding points with closest features. For example, for a point  $p$  with feature  $f_p$  in the mesh point cloud, its corresponding point  $p_q$  with feature  $f_q$  on the scene point cloud  $P_{scn}$  can be found by  $q_p = \operatorname{argmin}_{q \in P_{scn}} D(f_p, f_q)$ , where  $D(p, q)$  is the function to calculate cosine distance. To eliminate false positives from the extracted correspondences, we follow [10] and utilize differentiable ratio test to recalculate the weights of each pairs (i.e.,  $w = 1 - \frac{D(p, q_{p,1})}{D(p, q_{p,2})}$ ) and select the top  $K$  pairs for pose and size fitting. We end up with a correspondence set  $\mathcal{C} = \{(p, q, w)_i : 1 \leq i \leq K\}$ .

#### 3.3.2 Geometric Fitting for Pose and Size Estimation

Given a set of correspondences  $\mathcal{C} = \{(p, q, w)_i : 1 \leq i \leq K\}$ , we can estimate the pose and scale parameters with the Umeyama algorithm [34]. The Umeyama algorithm calculates the pose and the scale parameters by minimizing the squared loss:

$$L_{umeyama} = \sum_{i=1}^K \|q_i - (sRp_i + T)\|_2^2. \quad (1)$$

where  $s$  denotes the scale,  $R$  the rotation matrix and  $T$  the translation vector.

### 3.4. Differentiable Mesh Rendering

In the first two steps, we have eliminated the shape, pose and scale inconsistency by differentiable shape deformation and registration. We introduce the differentiable mesh rendering to eliminate the final partial-to-complete inconsistency. We first scale and transform the deformed normalized mesh from the object coordinate system to the camera coordinate system. We then utilize a differentiable renderer [30] to render the depth image. Finally, we lift the valid values in the depth image back to a point cloud with the given camera intrinsic matrix to obtain the predicted visible object point cloud. In this way, the partial to complete inconsistency is eliminated. To supervise our whole framework, we can enforce the geometric consistency between the predicted and the observed scene point cloud.



### 3.5. Regularizations

We apply three loss functions to regularize the learning of shape deformation.

**Deformed Shape Loss.** Chamfer distances [11, 41] is applied to regularize the shape deformation. One approach is to utilize point cloud sampled from the ground truth mesh for full supervision. While we want to eliminate the reliance on high-cost precise object mesh models, we utilize coarse object point clouds for weak supervision. The coarse object point cloud is obtained from several real RGBD images of the target object placed on marker boards in different views, which are then aggregated to a whole object point cloud and normalized to the same scale as the template mesh for weak supervision. Given the coarse point cloud  $P_T$  of the target object and the point cloud  $P_D$  differentially sampled [41] from the deformed mesh, the Chamfer distance can be calculated by:

$$L_{cd} = \sum_{p_1 \in P_T} \min_{p_2 \in P_D} \|p_1 - p_2\|_2^2 + \sum_{p_2 \in P_D} \min_{p_1 \in P_T} \|p_2 - p_1\|_2^2, \quad (2)$$

**Mesh Laplacian Loss.** Following 3DN [41], we apply laplacian loss to restrict smooth deformation across the mesh surface and preserve geometric details:

$$L_{lpc} = \sum_i \|Lpc(M) - Lpc(M^*)\|_2, \quad (3)$$

where  $Lpc$  denotes mesh Laplacian operator,  $M$  the original mesh and  $M^*$  the deformed one.

**Mesh Normal Consistency Loss.** To ensure the smoothness of the deformed mesh, a mesh normal consistency loss [30] is also applied:

$$L_{nc} = \sum_{n_0 \in N} \sum_{n_1 \in N} \mathbb{I}(n_0, n_1) \cdot (1 - \cos(n_0, n_1)), \quad (4)$$

where  $N$  denotes normal vectors of mesh faces.  $\mathbb{I}$  is an indication function equates to 1 when two normal vectors are from two neighboring faces, and 0 otherwise.

The total loss for regularization of shape deform is a weighted sum of the above three losses:

$$L_{df} = \lambda_{cd}L_{cd} + \lambda_{lpc}L_{lpc} + \lambda_{nc}L_{nc}. \quad (5)$$

where  $\lambda_*$  denotes the weight of the corresponding loss.

We apply geometric consistency loss and correspondence loss to regularize the learning of the pose and scale prediction network.

**Geometric Consistency Loss.** We utilize Chamfer distances to measure the geometric consistency between the predicted point cloud  $P_{pred}$  and the observed scene point cloud  $P_{scn}$ . The calculation is similar to Equation 2 and we denote the geometric consistency loss as  $L_{geo}$ .

**Correspondence Loss.** Following [10], we also apply weighted correspondence loss to enforce better correspondence exploring. Given the predicted correspondence sets  $\mathcal{C} = \{(p, q, w)_i, 1 \leq i \leq K\}$  and the estimated scale and pose parameters  $(s, R, T)$ , the weighted correspondence loss is defined as:

$$L_{w\_corr} = \frac{1}{K} \sum_{i=1}^K w_i \|q_i - (sRp_i + T)\|_2^2, \quad (6)$$

We obtain the total loss functions for registration with a weighted sum of the above three losses as follows:

$$L_{pose} = \lambda_{geo}L_{geo} + \lambda_{w\_corr}L_{w\_corr}. \quad (7)$$

where  $\lambda_*$  denotes the weight of each loss.

## 4. Experiments

### 4.1. Benchmark Datasets

**NOCS-REAL** [38] is a real-world dataset collected for category-level object pose and size estimation. It contains six categories of hand-scale objects, with six unique instances each. Real-world images of 13 scenes are captured, with 4300 images of 7 scenes for training and 2750 images of 6 scenes for evaluation. The cluttered scenes and variety of object shapes make the dataset challenging.

**YCB-Video** [2] is a popular benchmark dataset for instance-level object pose estimation. Following [37], we select five typical objects from the dataset and split the training and testing set as in [43, 36, 14].

### 4.2. Evaluation Metrics

For category-level pose and size estimation, we follow previous works [38, 6] and adopt the average precision of Intersection-over-Union (IoU) and  $n^\circ mcm$  as our evaluation metric. The  $IoU_x$  metrics evaluate pose and size entangled 3D object detection performance, with  $x \in \{25\%, 50\%, 75\%\}$  different acceptance IoU threshold. The pose-only  $D^\circ Mcm$  metric evaluates the performance of 6D pose estimation. The prediction is considered accurate when the rotation error is less than  $D^\circ$  and the translation error is less than  $M$  center meter. For symmetrical object categories, the rotation error around the symmetry axis is ignored. For instance-level 6D pose estimation, we follow [43, 14, 13] and report the ADD-S AUC (area under the accuracy-threshold curve) metric for symmetrical objects and ADD AUC for non-symmetrical ones.

### 4.3. Training and Implementation

**Network architecture.** We apply the part segmentation version of the 3DGCN [26] and PointNet++ [28]. Each Linear Transformer network [40] has 4 attention heads.

<sup>1</sup><https://github.com/mentian/object-deformnet>

Learning Scheme	Method	Training Data			Metrics $\uparrow$						
		real	syn.	type	$IoU_{25}$	$IoU_{50}$	$IoU_{75}$	$5^\circ 2cm$	$5^\circ 5cm$	$10^\circ 2cm$	$10^\circ 5cm$
Fully-Supervised	SPGA [5]	✓	✓	R&D	-	80.1	61.9	35.9	39.6	61.3	70.7
	DualPoseNet [25]	✓	✓	R&D	-	79.8	62.2	29.3	35.9	50.0	66.8
	FS-Net [6]	✓		D	-	92.2	63.5	-	28.2	-	64.6
	CASS [4]	✓	✓	R&D	-	77.7	-	-	23.5	-	58.0
	SPD [32]	✓	✓	R&D	83.0	77.3	53.2	19.3	21.4	43.2	54.1
	NOCS [38]	✓	✓	R&D	84.9	80.5	-	-	9.5	-	26.7
	SPD* [32]	✓		R&D	82.8	63.3	39.2	3.6	4.8	19.0	26.0
	NOCS [38]	✓		R&D	61.9	47.5	-	-	6.5	-	18.5
Traditional	ICP [1]			D	60.2	43.8	6.3	0.2	1.8	0.7	2.1
Self-Supervised	Ours-P	✓		D	76.1	34.1	8.1	0.4	1.8	0.5	11.9
	Ours-M	✓		D	83.5	58.7	32.0	4.7	5.6	13.7	17.4
	Ours-M + ICP [1]	✓		D	83.2	65.0	38.6	17.9	25.0	28.0	42.6

Table 1: Quantitative results on the NOCS-REAL dataset. Our self-supervised depth-only framework outperforms traditional ICP and some fully-supervised algorithms. syn.: synthesis data; R&D: RGBD; D: depth only; Ours-P: point-based; Ours-M: mesh-based; -: results not reported. SPD\*: We use the official code<sup>1</sup> of SPD and train on REAL275 for 50 epochs as ours.

	SPD [32]	SGPA [5]	TPM	3DN [41]	Ours /MS	Ours
shape	PC	PC	Mesh	Mesh	Mesh	Mesh
bottle	4.34	2.93	6.21	3.90	2.41	<b>2.21</b>
bowl	1.21	0.89	0.88	0.98	0.66	<b>0.55</b>
camera	8.30	<b>5.51</b>	9.95	7.30	6.24	5.81
can	1.80	1.75	3.15	1.83	1.82	<b>1.70</b>
laptop	2.10	1.62	4.39	1.81	1.14	<b>0.97</b>
mug	1.06	1.12	0.88	1.10	0.98	<b>0.77</b>
mean	2.99	2.44	4.24	2.82	2.21	<b>2.00</b>

Table 2: Quantitative results of shape deformation in the Chamfer Distance metric  $\downarrow (\times 10^{-3})$ . TPM: category template mesh to be deformed; /MS: without multi-scale geometry enhancement; PC: point cloud.

Object ID	1	2	5	10	15	Mean
Template	5.91	6.31	3.15	3.31	4.73	4.68
Ours	0.18	0.18	0.12	0.09	0.13	0.14

Table 3: Quantitative results of shape deformation in the Chamfer Distance metric  $\downarrow (\times 10^{-3})$  on YCB-Video.

**Training details.** We first train the mesh deformation network then fix the weight and train the registration network. We train each network with Adam [21] optimizer by 50 epochs. The initial learning rate is  $1e-4$  for deformation network and  $2e-5$  for registration, and are halved every 10 epochs. We empirically set  $\lambda_{cd}$ ,  $\lambda_{lpc}$ ,  $\lambda_{nc}$  to be 3, 0.1, 0.01 in Formula 5 and  $\lambda_{geo}$ ,  $\lambda_{w_{corr}}$  to be 10, 0.1 in Formula 7.

Object ID	1	2	5	10	15	Mean
ICP	17.3	17.6	32.6	25.9	24.0	23.5
Ours	<b>74.8</b>	<b>66.5</b>	<b>83.0</b>	<b>80.9</b>	<b>68.2</b>	<b>74.7</b>

Table 4: Quantitative results of 6D object pose on the deformed YCB-Video dataset (ADD(S) AUC  $\uparrow$  [13, 43]).

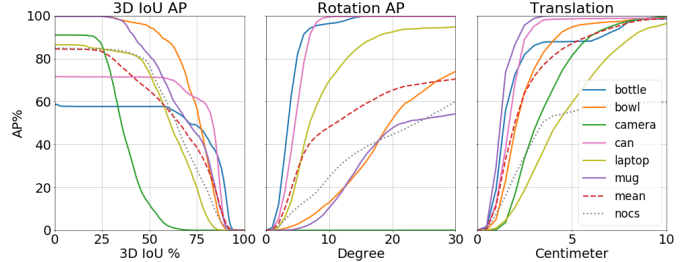


Figure 3: Results of our refined pipeline on the NOCS-REAL test set. The average precision of 3D IoU, rotation and translation in different thresholds are reported.

#### 4.4. Evaluation on Benchmark Datasets

**Category-level pose and size estimation.** Table 1 shows the quantitative evaluation results on the NOCS-REAL dataset. We compare our self-supervised framework with existing fully-supervised ones. Besides, we apply ICP on the template mesh as a simple baseline that doesn't require ground truth pose labels. As shown in the table, our mesh-based self-supervised approach (Ours-M) surpasses ICP by a large margin, i.e. +25.7% on  $IoU_{25}$  and +15.3% on  $10^\circ 5cm$ . We also obtained competitive or even better results against some supervised approaches that only train

Method	Module			Metrics	
	DEF.	REG.	REN.	$IoU_{50} \uparrow$	$5^\circ 5cm \uparrow$
Ours		✓	✓	45.3	2.6
Ours	✓		✓	40.5	1.9
Ours	✓	✓		54.3	4.8
Ours	✓	✓	✓	<b>58.7</b>	<b>5.6</b>
ICP				43.8	1.8
Ours+ICP	✓			48.7	4.8
Ours+ICP	✓	✓		59.2	10.4
Ours+ICP	✓	✓	✓	<b>65.0</b>	<b>25.0</b>

Table 5: Effect of each component in our pipeline. They are designed to disentangle different inconsistencies and benefits not only our self-supervised pipeline, but also the traditional ICP algorithm. DEF.: Deformation; REG.: Registration; REN.: Rendering.

on real data as ours, i.e. +21.6% on  $IoU_{25}$  compared with NOCS [38] and +0.8% on  $5^\circ 5cm$  compared with SPD [32]. Amazingly, since our full framework is designed to eliminate the entangled shape, pose, scale, and partial to complete inconsistencies between the category template shape and the scene point cloud, we find applying simple ICP on our rendered depth and the scene point cloud further improve the accuracy by large margins, proving the efficacy of our network to eliminate these challenging inconsistencies. Moreover, our ICP refined version shows the possibility of eradicating labor-intensive pose labels for training as it already surpasses many recently proposed fully-supervised methods (i.e. NOCS-2019, SPD-2020, CASS-2020) on the strict  $5^\circ 5cm$  metric! Detailed results are in Figure 3. Some qualitative results are shown in Figure 4.

**Shape deformation.** For mesh deformation, we choose the mesh from ShapeNet [3] with smallest CD distance to the prior point shape in SPD [32] as template mesh (TPM). As shown in Table 2, our pose- and scale-invariant shape deformation network advances the 3DN [41] baseline by 29% on shape deformation and also outperforms point cloud baselines.

**Shape deformation and pose estimation on the YCB-Video.** We first add noises to the provided CAD models by box-cage deformation in FS-Net [6] to be templates. We mask out object point clouds from the scene with ground truth segmentation. Results of our shape deformation and pose estimation are shown in Table 3 & 4 respectively.

#### 4.5. Ablation Study

In this subsection, we present extensive ablation studies on our design choices and discuss their effect.

**Effect of the deformation, registration, and rendering module.** In Table 5, we ablate different modules to study their effect. As shown in the table, for our frame-

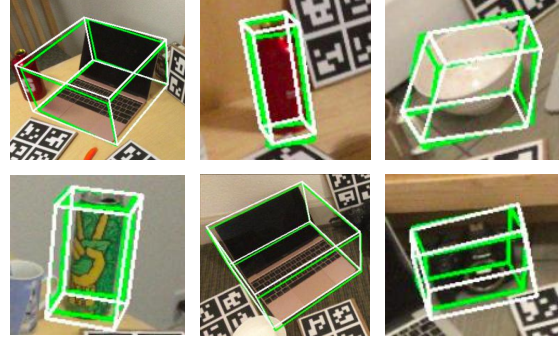


Figure 4: Qualitative results on NOCS-REAL. The predicted poses are in green and the ground truths in white.

work, the deformation step eliminates the shape inconsistency and contributes 13.4% mAP improvement on  $IoU_{50}$  and 3% on  $5^\circ 5cm$ . The registration step eliminates pose and scale inconsistencies and outperforms direct pose regression (+18.2% on  $IoU_{50}$ , +3.7% on  $5^\circ 5cm$ ). Finally, the rendering module further eases the partial to complete inconsistency and advances the performance (+4.4% on  $IoU_{50}$ , +0.8% on  $5^\circ 5cm$ ). Besides, we further utilize ICP to validate the efficacy of each module in our pipeline for inconsistency elimination. The performance of ICP depends much on the initialization, which means it's sensitive to the shape, pose, scale, and partial-to-complete inconsistency between the two input point clouds. As shown in the table, when the above inconsistencies are eased by our framework step by step, the performance of ICP also improves progressively, proving the efficacy of each component.

**Effect of multi-scale geometry enhancement.** As shown in Table 2, the proposed multi-scale geometry enhancement improves the deformation result by 9.5%.

**Effect of Linear Transformers to point cloud registration.** Compared to the original GNN and vanilla transformers version in PREDATOR [16], our version gets +1.3% improvement on  $IoU_{75}$  AP $\uparrow$  for pose and scale estimation.

**Is the shape deformation pose and scale-invariant?** Yes. We transform the partial scene point cloud to the same pose and scale as the template mesh as inputs and then train the mesh deformation network, getting 1.98 mean CD distance, vs. 2.00 from pose- and scale-inconsistent inputs.

**Point-based or mesh-based approaches?** Some works deform shape [32, 5] or render depth [10] from point cloud. We implement a point-based version for comparison. Specifically, we randomly sample 2048 points from the mesh as template shape, remove losses denoted in Equation 3 & 4, use a point renderer, and keep the rest as our mesh-based approach. We compare point-based (Ours-P) and mesh-based (Ours-M) pipelines in Table 1, finding the sparse point cloud cause artifacts on the rendered depth, and the partial-to-complete inconsistency is not well eliminated, which cause big performance drop.



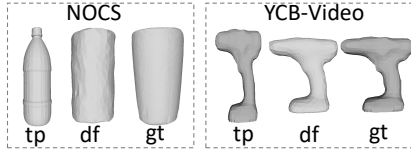


Figure 5: Qualitative results on mesh deformation. tp: template; df: deformed; gt: ground truth.

## 5. Discussion and Limitations

We propose a novel self-supervised framework for category-level pose and size estimation via differentiable shape deformation, registration, and rendering. Thanks to the elimination of the challenging shape, pose, scale, and partial to complete inconsistencies, our refined pipeline outperforms traditional algorithms and some of the fully-supervised ones, showing the possibility of eradicating the labor-intensive ground truth labels. However, there are still limitations in this work. Firstly, we rely on a segmentation network to segment out regions of interest from the captured scene. A unified framework will be more practical. Secondly, though the requirement of ground truth pose and size labels are eradicated, a coarse target object point cloud is still required to weakly supervise our shape deformation network. One future direction is to eliminate this dependency. Lastly, despite good results, there is still a performance gap between self-supervised and fully-supervised algorithms. We expect more future research to bridge the gap.

## References

- [1] Paul J Besl and Neil D McKay. Method for registration of 3-d shapes. In *Sensor fusion IV: control paradigms and data structures*, volume 1611, pages 586–606. International Society for Optics and Photonics, 1992. 1, 7
- [2] Berk Calli, Arjun Singh, Aaron Walsman, Siddhartha Srinivasa, Pieter Abbeel, and Aaron M Dollar. The ycb object and model set: Towards common benchmarks for manipulation research. In *2015 international conference on advanced robotics (ICAR)*, pages 510–517. IEEE, 2015. 6
- [3] Angel X Chang, Thomas Funkhouser, Leonidas Guibas, Pat Hanrahan, Qixing Huang, Zimo Li, Silvio Savarese, Manolis Savva, Shuran Song, Hao Su, et al. Shapenet: An information-rich 3d model repository. *arXiv preprint arXiv:1512.03012*, 2015. 8
- [4] Dengsheng Chen, Jun Li, Zheng Wang, and Kai Xu. Learning canonical shape space for category-level 6d object pose and size estimation. In *Proceedings of the IEEE/CVF conference on computer vision and pattern recognition*, pages 11973–11982, 2020. 1, 2, 7
- [5] Kai Chen and Qi Dou. Sgpa: Structure-guided prior adaptation for category-level 6d object pose estimation. In *Proceedings of the IEEE/CVF International Conference on Computer Vision (ICCV)*, pages 2773–2782, October 2021. 1, 2, 7, 8
- [6] Wei Chen, Xi Jia, Hyung Jin Chang, Jinming Duan, Linlin Shen, and Ales Leonardis. Fs-net: Fast shape-based network for category-level 6d object pose estimation with decoupled rotation mechanism. In *Proceedings of the IEEE/CVF Conference on Computer Vision and Pattern Recognition*, pages 1581–1590, 2021. 1, 2, 4, 6, 7, 8
- [7] Xiaozhi Chen, Huimin Ma, Ji Wan, Bo Li, and Tian Xia. Multi-view 3d object detection network for autonomous driving. In *Proceedings of the IEEE Conference on Computer Vision and Pattern Recognition*, pages 1907–1915, 2017. 1
- [8] Alvaro Collet, Manuel Martinez, and Siddhartha S Srinivasa. The moped framework: Object recognition and pose estimation for manipulation. *The International Journal of Robotics Research*, 30(10):1284–1306, 2011. 1
- [9] Dorin Comaniciu and Peter Meer. Mean shift: A robust approach toward feature space analysis. *IEEE Transactions on Pattern Analysis & Machine Intelligence*, (5):603–619, 2002.
- [10] Mohamed El Banani, Luya Gao, and Justin Johnson. Unsupervisedr: Unsupervised point cloud registration via differentiable rendering. In *Proceedings of the IEEE/CVF Conference on Computer Vision and Pattern Recognition*, pages 7129–7139, 2021. 3, 5, 6, 8
- [11] Haoqiang Fan, Hao Su, and Leonidas J Guibas. A point set generation network for 3d object reconstruction from a single image. In *Proceedings of the IEEE conference on computer vision and pattern recognition*, pages 605–613, 2017. 6
- [12] Andreas Geiger, Philip Lenz, and Raquel Urtasun. Are we ready for autonomous driving? the kitti vision benchmark suite. In *2012 IEEE Conference on Computer Vision and Pattern Recognition*, pages 3354–3361. IEEE, 2012. 1
- [13] Yisheng He, Haibin Huang, Haoqiang Fan, Qifeng Chen, and Jian Sun. Ffb6d: A full flow bidirectional fusion network for 6d pose estimation. In *Proceedings of the IEEE/CVF Conference on Computer Vision and Pattern Recognition*, pages 3003–3013, 2021. 1, 6, 7
- [14] Yisheng He, Wei Sun, Haibin Huang, Jianran Liu, Haoqiang Fan, and Jian Sun. Pvn3d: A deep point-wise 3d keypoints voting network for 6dof pose estimation. In *Proceedings of the IEEE/CVF Conference on Computer Vision and Pattern Recognition*, pages 11632–11641, 2020. 1, 6
- [15] Tomáš Hodan, Pavel Haluza, Štěpán Obdržálek, Jiri Matas, Manolis Lourakis, and Xenophon Zabulis. T-less: An rgb-d dataset for 6d pose estimation of texture-less objects. In *2017 IEEE Winter Conference on Applications of Computer Vision (WACV)*, pages 880–888. IEEE, 2017. 1
- [16] Shengyu Huang, Zan Gojcic, Mikhail Usvyatsov, Andreas Wieser, and Konrad Schindler. Predator: Registration of 3d point clouds with low overlap. In *Proceedings of the IEEE/CVF Conference on Computer Vision and Pattern Recognition*, pages 4267–4276, 2021. 3, 5, 8
- [17] Du Q Huynh. Metrics for 3d rotations: Comparison and analysis. *Journal of Mathematical Imaging and Vision*, 35(2):155–164, 2009.
- [18] Dominic Jack, Jhony K Pontes, Sridha Sridharan, Clinton Fookes, Sareh Shirazi, Frederic Maire, and Anders Eriksson.

- Learning free-form deformations for 3d object reconstruction. In *Asian Conference on Computer Vision*, pages 317–333. Springer, 2018. 2
- [19] Chiyu Jiang, Jingwei Huang, Andrea Tagliasacchi, Leonidas Guibas, et al. Shapeflow: Learnable deformations among 3d shapes. *arXiv preprint arXiv:2006.07982*, 2020. 2
- [20] Roman Kaskman, Sergey Zakharov, Ivan Shugurov, and Slobodan Ilic. Homebreweddb: Rgb-d dataset for 6d pose estimation of 3d objects. In *Proceedings of the IEEE/CVF International Conference on Computer Vision Workshops*, pages 0–0, 2019. 1
- [21] Diederik P Kingma and Jimmy Ba. Adam: A method for stochastic optimization. *arXiv preprint arXiv:1412.6980*, 2014. 7
- [22] Alexander Krull, Eric Brachmann, Frank Michel, Michael Ying Yang, Stefan Gumhold, and Carsten Rother. Learning analysis-by-synthesis for 6d pose estimation in rgb-d images. In *Proceedings of the IEEE international conference on computer vision*, pages 954–962, 2015. 2
- [23] Andrey Kurenkov, Jingwei Ji, Animesh Garg, Viraj Mehta, JunYoung Gwak, Christopher Choy, and Silvio Savarese. Deformnet: Free-form deformation network for 3d shape reconstruction from a single image. In *2018 IEEE Winter Conference on Applications of Computer Vision (WACV)*, pages 858–866. IEEE, 2018. 2
- [24] Xiaolong Li, Yijia Weng, Li Yi, Leonidas Guibas, A Lynn Abbott, Shuran Song, and He Wang. Leveraging se (3) equivariance for self-supervised category-level object pose estimation. *arXiv preprint arXiv:2111.00190*, 2021. 2
- [25] Jiehong Lin, Zewei Wei, Zhihao Li, Songcen Xu, Kui Jia, and Yuanqing Li. Dualposenet: Category-level 6d object pose and size estimation using dual pose network with refined learning of pose consistency. In *Proceedings of the IEEE/CVF International Conference on Computer Vision (ICCV)*, pages 3560–3569, October 2021. 2, 7
- [26] Zhi-Hao Lin, Sheng-Yu Huang, and Yu-Chiang Frank Wang. Convolution in the cloud: Learning deformable kernels in 3d graph convolution networks for point cloud analysis. In *Proceedings of the IEEE/CVF Conference on Computer Vision and Pattern Recognition*, pages 1800–1809, 2020. 3, 4, 6
- [27] Eric Marchand, Hideaki Uchiyama, and Fabien Spindler. Pose estimation for augmented reality: a hands-on survey. *IEEE transactions on visualization and computer graphics*, 22(12):2633–2651, 2015. 1
- [28] Charles Ruizhongtai Qi, Li Yi, Hao Su, and Leonidas J Guibas. Pointnet++: Deep hierarchical feature learning on point sets in a metric space. In *Advances in neural information processing systems*, pages 5099–5108, 2017. 5, 6
- [29] B Ravani and B Roth. Motion synthesis using kinematic mappings. 1983.
- [30] Nikhila Ravi, Jeremy Reizenstein, David Novotny, Taylor Gordon, Wan-Yen Lo, Justin Johnson, and Georgia Gkioxari. Accelerating 3d deep learning with pytorch3d. *arXiv preprint arXiv:2007.08501*, 2020. 5, 6
- [31] Martin Sundermeyer, Zoltan-Csaba Marton, Maximilian Durner, and Rudolph Triebel. Augmented autoencoders: Implicit 3d orientation learning for 6d object detection. *International Journal of Computer Vision*, 128(3):714–729, 2020. 2
- [32] Meng Tian, Marcelo H Ang, and Gim Hee Lee. Shape prior deformation for categorical 6d object pose and size estimation. In *European Conference on Computer Vision*, pages 530–546. Springer, 2020. 1, 2, 7, 8
- [33] Jonathan Tremblay, Thang To, Balakumar Sundaralingam, Yu Xiang, Dieter Fox, and Stan Birchfield. Deep object pose estimation for semantic robotic grasping of household objects. *arXiv preprint arXiv:1809.10790*, 2018. 1
- [34] Shinji Umeyama. Least-squares estimation of transformation parameters between two point patterns. *IEEE Transactions on Pattern Analysis & Machine Intelligence*, 13(04):376–380, 1991. 5
- [35] Ashish Vaswani, Noam Shazeer, Niki Parmar, Jakob Uszkoreit, Llion Jones, Aidan N Gomez, Łukasz Kaiser, and Illia Polosukhin. Attention is all you need. In *Advances in neural information processing systems*, pages 5998–6008, 2017. 4
- [36] Chen Wang, Danfei Xu, Yuke Zhu, Roberto Martín-Martín, Cewu Lu, Li Fei-Fei, and Silvio Savarese. Densefusion: 6d object pose estimation by iterative dense fusion. In *Proceedings of the IEEE Conference on Computer Vision and Pattern Recognition*, pages 3343–3352, 2019. 6
- [37] Gu Wang, Fabian Manhardt, Jianzhun Shao, Xiangyang Ji, Nassir Navab, and Federico Tombari. Self6d: Self-supervised monocular 6d object pose estimation. In *European Conference on Computer Vision*, pages 108–125. Springer, 2020. 1, 2, 6
- [38] He Wang, Srinath Sridhar, Jingwei Huang, Julien Valentin, Shuran Song, and Leonidas J Guibas. Normalized object coordinate space for category-level 6d object pose and size estimation. In *Proceedings of the IEEE Conference on Computer Vision and Pattern Recognition*, pages 2642–2651, 2019. 1, 2, 6, 7, 8
- [39] Jiaze Wang, Kai Chen, and Qi Dou. Category-level 6d object pose estimation via cascaded relation and recurrent reconstruction networks. *arXiv preprint arXiv:2108.08755*, 2021. 2
- [40] Sinong Wang, Belinda Z Li, Madian Khabza, Han Fang, and Hao Ma. Linformer: Self-attention with linear complexity. *arXiv preprint arXiv:2006.04768*, 2020. 3, 4, 6
- [41] Weiyue Wang, Duygu Ceylan, Radomir Mech, and Ulrich Neumann. 3dn: 3d deformation network. In *Proceedings of the IEEE/CVF Conference on Computer Vision and Pattern Recognition*, pages 1038–1046, 2019. 2, 4, 5, 6, 7, 8
- [42] Yue Wang, Yongbin Sun, Ziwei Liu, Sanjay E Sarma, Michael M Bronstein, and Justin M Solomon. Dynamic graph cnn for learning on point clouds. *Acm Transactions On Graphics (tog)*, 38(5):1–12, 2019. 5
- [43] Yu Xiang, Tanner Schmidt, Venkatraman Narayanan, and Dieter Fox. Posecnn: A convolutional neural network for 6d object pose estimation in cluttered scenes. *arXiv preprint arXiv:1711.00199*, 2017. 6, 7
- [44] Danfei Xu, Dragomir Anguelov, and Ashesh Jain. Pointfusion: Deep sensor fusion for 3d bounding box estimation. In *Proceedings of the IEEE Conference on Computer Vision and Pattern Recognition*, pages 244–253, 2018. 1

- [45] Wang Yifan, Noam Aigerman, Vladimir G Kim, Siddhartha Chaudhuri, and Olga Sorkine-Hornung. Neural cages for detail-preserving 3d deformations. In *Proceedings of the IEEE/CVF Conference on Computer Vision and Pattern Recognition*, pages 75–83, 2020. [2](#), [4](#)
- [46] M Ersin Yumer and Niloy J Mitra. Learning semantic deformation flows with 3d convolutional networks. In *European Conference on Computer Vision*, pages 294–311. Springer, 2016. [2](#)